ELSEVIER

October 1995

Optical Materials 4 (1995) 823–831

OPTICAL Materials

Surface polish characterization of industrial Ti:sapphire laser crystal rods by photopyroelectric scanning imaging

J. Shen [a], K. Fjeldsted [b], J. Vanniasinkam [a], A. Mandelis [a]

[a] *Photothermal and Optoelectronic Diagnostics Laboratory, Department of Mechanical Engineering, University of Toronto, Toronto, M5S 1A4, Canada*

[b] *Crystar Research Inc., Victoria, B.C., V8Z 3B6, Canada*

Received 26 April 1995; accepted 16 June 1995

Abstract

Photopyroelectric scanning imaging of a Ti:sapphire crystal with three different surface polishes was carried out using a novel non-contact experimental configuration. Bulk optical absorption coefficient, surface optical absorptance and theoretically normalized quadrature (Q) signal images were obtained. In addition to growth defects in the crystal, the photothermal Q images revealed variations due to the quality of surface polishes in terms of surface optical absorptance, and thermal resistance and homogeneity of each polish. Purely optical-transmission scanned images exhibited lower sensitivity to the degree of the defective state of the Ti:sapphire rod surface due to polishing. It is concluded that photopyroelectric scanning imaging can be used in the quality control of both crystal growth and surface processing of Ti:sapphire crystals.

1. Introduction

In recent years, a novel non-contact photopyroelectric spectroscopic (PPES) configuration, shown as Fig. 1, has been developed to study Ti:sapphire (Ti^{3+}:Al_2O_3) laser crystals with widely different figures of merit [1]. By varying the air layer thickness L, high-resolution spectra of optical-to-thermal energy conversion efficiency, $\eta_{NR}(\lambda)$, and optical absorption coefficient, $\beta(\lambda)$, can be simultaneously measured from lock-in quadrature (Q) and in-phase (IP) PPES signals, respectively. With this spectrometer and a monolithic PPES theoretical model [1], absolute non-radiative-energy-conversion-efficiency scanning imaging has also been successfully carried out to map the optical quality of growth defect regions in Ti:sapphire crystals [2].

It has been found [1] that surface absorption layers on a Ti:sapphire crystal convert the absorbed optical energy into heat much more efficiently than bulk regions, thus significantly decreasing the overall lumi-

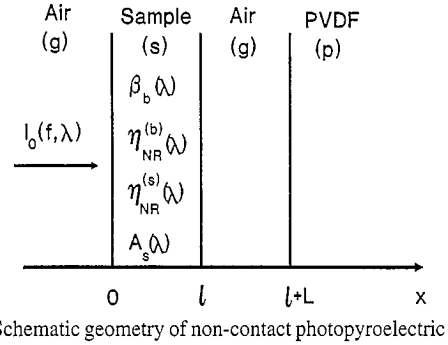

Fig. 1. Schematic geometry of non-contact photopyroelectric (PPE) imaging of a transparent sample of thickness l, bulk optical absorption coefficient $\beta_b(\lambda)$, surface optical absorptance $A_s(\lambda)$, bulk non-radiative energy conversion efficiency $\eta_{NR}^{(b)}(\lambda)$, and surface non-radiative energy conversion efficiency $\eta_{NR}^{(s)}(\lambda)$. Air-layer thickness is L; semi-infinite polyvinylidene fluoride (PVDF) pyroelectric detector; optical modulation frequency f; incident optical intensity I_0.

SSDI 0925-3467(95)00025-9

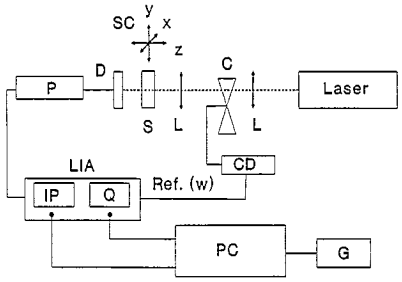

Fig. 2. Schematic of non-contact PPE scanning imager. L: lens, C: chopper, SC: (x, y, z) scanning accessory, D: Polyvinyl Fluoride (PVDF) pyroelectric detector, S: sample, P: preamplifier, CD: chopper driver, LIA: lock-in amplifier (in IP or Q mode), PC: computer for data acquisition, processing and analysis, G: graphics and plotter.

nescence efficiency of the crystal. These so-called non-radiative surface layers (NRSLs), which can cause severe optical losses, are most likely the result of mechanical polishing of the crystals, which occurs during surface processing of manufactured laser rods. It is therefore important to improve the surface treatment processes before committing significant resources to the harder task of enhancing the bulk optical quality of Ti:sapphire crystals through costly modifications in the crystal growth process.

Contribution to PPES signals from surface layers provides information on the optical quality of surfaces of optical/laser materials. Such information can be obtained by de-convolution of bulk and surface contributions using two crystals of identical properties and different thicknesses with the help of an extended theoretical model [3]. In this paper, we report the scanning imaging of Ti:sapphire crystal wafers with three different polishes using the PPE scanning spectrometer of Fig. 2. The comparison between purely optical (IP) PPE scans and thermal-wave (Q) scans revealed the enhanced sensitivity of the latter and the usefulness of the technique in the quality control of surface polishing of laser materials.

2. Theoretical background

According to the experimental geometry of the non-contact PPES technique, Figs. 1 and 2, the distance between sample and detector, L, namely the air layer thickness, can be varied. When $L \to \infty$, i.e. the air layer thickness is much larger than the thermal diffusion length [4] (0.89 mm in air, when modulation frequency is 9 Hz), then no thermal wave energy reaches the detector and the quadrature signal in the lock-in amplifier is essentially zero [1]. In practice, $L \approx 5$ mm suffices to satisfy the $L \to \infty$ condition. Under this condition (named the "purely optical" mode), the pyroelectric detector (usually a polyvinylidene fluoride (PVDF) thin film) plays the role of a conventional optical transmission sensor, generating a PPE signal proportional to the intensity of the radiation transmitted through the thickness on a crystal of an optical material. The IP signal can therefore be used for the calculation of the bulk optical absorption coefficient, $\beta_b(\lambda)$, and surface layer optical absorptance, $A_s(\lambda)$, in this purely optical mode [3]:

$$\beta_b l + 2A_s = -\ln\left(\frac{(1-R_s)^2}{2R_s^2\rho_\infty}\left\{\left[1 + \left(\frac{2\rho_\infty R_s}{(1-R_s)^2}\right)^2\right]^{1/2} - 1\right\}\right), \quad (1a)$$

where

$$\rho_\infty(\lambda) \equiv V_\infty(\lambda)/V_R(\lambda)\,. \quad (1b)$$

V_∞ represents the PPE signal with the sample at $L \to \infty$; V_R is the PPE signal without the sample in place, a normalizing reference signal; l is the thickness of the sample; and $R_s(\lambda)$ is the surface reflectance of the sample. With two crystals of identical properties and different thicknesses, l_1 and l_2, Eq. (1a) is valid for each one of the two crystals. $\beta_b(\lambda)$ and $A_s(\lambda)$ can then be obtained by solving these two equations at each spectral wavelength λ.

When the air layer thickness L is decreased to a distance less than the thermal diffusion length in the air, in addition to the transmitted optical signal, the PVDF detector detects the thermal wave generated in the sample. In this thermo-optical mode, both IP and Q signals appear and the optical-to-thermal energy conversion efficiency can be calculated using the Q signal, theoretically corresponding to [3]

$$S_Q(\lambda) = \mathrm{Im}[V_L(\lambda)/V_R(\lambda)]\,, \quad (2)$$

where V_L indicates the PPE signal at an air layer thickness $L < \infty$.

3. Materials, experimental and results

In the PPE scanning imaging configuration of Fig. 2, a 10 mW He-Ne laser (632.8 nm) was used. This

photothermal source is more stable and intense than the monochromatized output of the Xe lamp used for PPE spectroscopy of Ti:sapphire crystals in this work and in our earlier studies [2]. After passing through two collimating lenses, the spot size of the He-Ne laser was expanded to 2 mm in diameter at the detector in order to satisfy the one dimensional treatment in the theoretical model [3], in which the spot size must be large compared to the thermal diffusion length in the sample. The samples were fixed on a scanning accessory, consisting of three micrometer stages, along the Cartesian coordinates, x, y and z. The purely optical mode was obtained by moving the sample along the z direction, so that $L=5$ mm. When L was reduced to ca. 0.2 mm, a Q signal was measurable in the thermo-optical mode. The PVDF detector was sooted to eliminate its optical reflection, and a chopping frequency $f=9$ Hz was used, yielding a near-optimal signal-to-noise ratio. It was noticed experimentally that when the radiation from the 99:1 linearly polarized He-Ne laser was incident onto a Ti:sapphire crystal sample parallel to the c-axis, the value of the photopyroelectric signal changed, if the sample were rotated around its axis. No such polarization phenomenon could be observed when the partially polarized Xe lamp and monochromator assembly was used for spectroscopic analysis. Furthermore, the normalized signal values, V_∞/V_R and V_L/V_R, were not the same as that when the laser was used, even if the wavelength of light were the same. This rotational dependence of the laser-induced PPE signal was used to fix the angular position for our samples so as to give excellent reproducibility and the maximum signal value when performing scanning imaging.

The Ti:sapphire crystals used in this work were grown by the Czochralski pulling technique from a molten mixture of Al_2O_3-Ti_2O_3. A pair of crystals of ca. 12 mm in diameter was utilized in order to measure $\beta_b(\lambda)$ and $A_s(\lambda)$, by use of Eq. (1). The crystals were cut from the same annealed boule. One was a long rod ($l \approx 20$ mm) and the other was a thin disk ($l \approx 2$ mm). These samples were subjected to three different sequential surface polishing processes, hereafter labelled polishes #1, 2 and 3. Polish #1 was the roughest one, and the resulting surface layer was thick and visibly nonhomogenous. Polish #2 was the result of grinding with diamond slurry containing 6 μm-size particulates, and was of much better quality than polish #1. Nevertheless, there remained some visible scratches, indicating

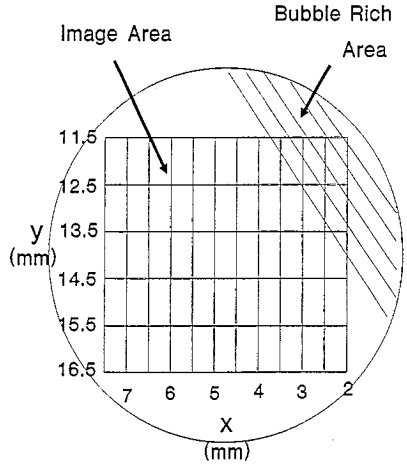

Fig. 3. Schematic of a cross section of the Ti:sapphire crystal used in scanning imaging, indicating imaging pixel configuration and density, scan coordinates, and bubble-rich area.

that the rough surface layer had not been thoroughly removed. Polish #3 was the result of grinding with diamond slurry containing 0.25 μm-size particulates: it was visually of the highest optically quality and homogeneity. After each surface polish (identical for both samples), PPE imaging scans were performed on the Ti:sapphire crystal pair, leading to the calculation of optical and photothermal parameters pertaining to that particular polish. The scanning imaging was supplemented with PPE spectroscopy of the crystal pair in the 350–1100 nm region. The crystals were subsequently polished further and PPE imaging and spectroscopy were repeated. For reasons of experimental convenience, thermo-optical scans at $L=0.2$ mm were performed only on the thin Ti:sapphire sample, following the determination of β_b(632.8 nm) and A_s(632.8 nm) from the pair of crystals through purely optical scans.

Fig. 3 shows the cross section of the thin sample. Along one region (upper right-hand quadrant) there was an area with a visibly high density of microbubbles. The rest of the crystal was clear. The line grid shown superposed on the crystal cross-section indicates the extent of the photopyroelectrically scanned region, as well as the approximate size and pixel density, resolution and coordinates of the PPE images. Both purely optical ($L \to \infty$) and thermal-wave ($L < \infty$) scans performed on this crystal with the optimal surface polish (#3) were obtained to check the effect of the microbubbles on the IP and Q channels of the PPE signal. The experimentally normalized IP and Q signals

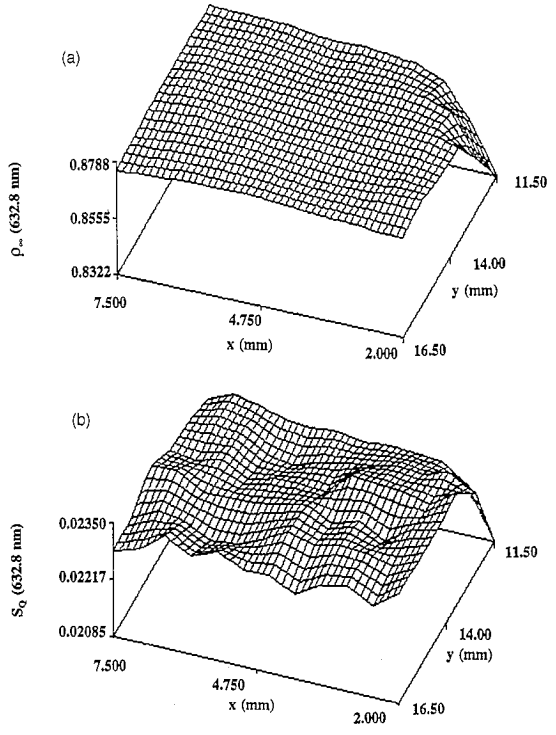

Fig. 4. Scanning imaging of experimentally normalized IP and Q signals of the Ti:sapphire crystal with (the best) polish #3. (a) IP signal, (b) Q signal, normalized by the optical power throughput of the 10 mW He-Ne laser source.

$\rho_\infty(632.8\ \text{nm})$ and $S_Q(632.8\ \text{nm})$, respectively, are shown in Fig. 4. Both images clearly exhibit the bubble-rich area, which resulted in enhanced light scattering and led to low IP and Q signals.

The roughness of polish #1 also caused a high degree of light scattering. Since the effects of surface scattering (which amounts to loss of photons) are not accounted for in Eqs. (1) and (2), these equations overestimate the value of the bulk optical absorption coefficient (net loss of photons) and underestimate the value of the quadrature signal (due to the eventual conversion of scattered photons to heat on the surface). Therefore, a correction for the scattered light has been made to Eqs. (1) and (2). As the presence of different surface polishes on the same crystal will not change the bulk optical absorption of the crystal, the difference of effective bulk optical absorption coefficients of the sample with polish #1 and polish #2 is due to light scattering by polish #1, resulting in less optical energy propagating through the sample. The light energy loss due to scattering by polish #1 is then $I_0(\beta_{b1}-\beta_{b2})l$, where I_0 is the incident optical intensity; β_{b1} and β_{b2} are the effective bulk optical absorption coefficients with polishes #1 and #2, respectively, obtained using Eq. (1), before taking the scattered light into account. Therefore, the corrected normalizing reference signal is equal to $V_R(\lambda)[\beta_{b1}(\lambda)-\beta_{b2}(\lambda)]$ instead of $V_R(\lambda)$ in Eqs. (1) and (2). Taking this scattered light loss into account, the bulk optical absorption coefficient and surface optical absorptance of the sample with polish #1 were obtained from the PPE data of the thick/thin crystal pair [3]. Fig. 5 shows the deconvoluted surface and bulk spectra obtained with the 1000 W Xe lamp from the Ti:sapphire crystal pair with surface polishes #1, #2 and #3. The bulk optical absorption peak in the visible region of Fig. 5a corresponds to the $^2T_{2g}\rightarrow{}^2E_g$ transition vibronically broadened by phonons [5]. The peak-shoulder formation in the 500-nm region is the overlap of a double hump due to a static Jahn-Teller distortion [6] of the E state, which splits the excited state by $\sim 2000\ \text{cm}^{-1}$. The optical absorption in the infrared area is generated by structural (point) defects associated with titanium ions [7,8] and

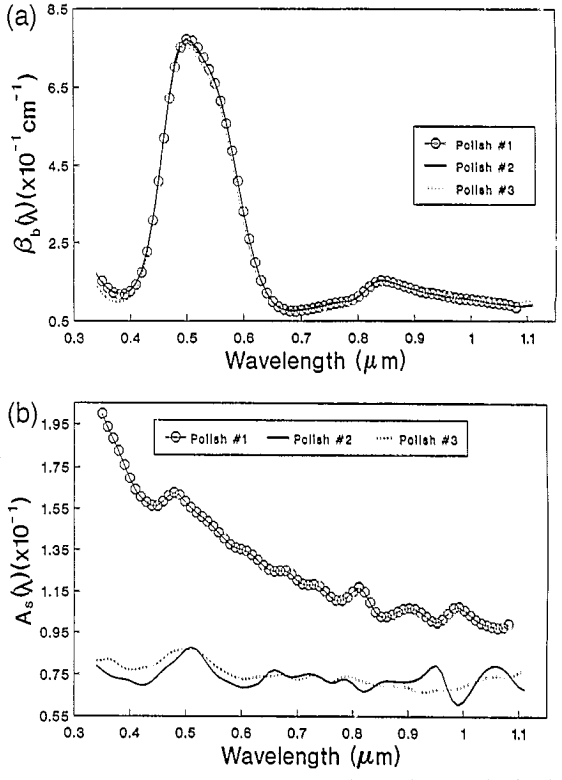

Fig. 5. Deconvoluted PPE spectra of the Ti:sapphire crystal pair with three polishes: (a) bulk optical absorption coefficient spectra, (b) surface optical absorptance spectra.

the relaxation of Ti^{3+} ions from interstitial or defect sites into Al^{3+} sites [6]. The bulk optical absorption coefficients, $\beta_b(\lambda)$, with the three different polishes very nearly coincide as expected, after accounting for light scattering due to polish #1. This result is indicative of the successful deconvolution of the surface and bulk contributions. The surface absorptance, Fig. 5b, of the polish #1 is, however, much higher than that of polishes #2 and #3, indicating a significant damage layer on the crystal surface. Even though both spectra due to polishes #2 and #3 are approximately similar in the range of the He-Ne laser emission, it is interesting to note that in 340–600 nm range the surface absorptance of polish #3 is slightly higher than that of polish #2. It can also be seen that all three surface spectra retain the main absorption peak of the Ti^{3+} ion in Al_2O_3 in the neighborhood of 500 nm. The peak corresponding to polish #1 (highest damage) is blue-shifted by by ca. 10 nm due to the steep absorption baseline.

Fig. 6 shows β_b(632.8 nm) images of the thin crystal, corresponding to Fig. 3 with different polishes. As expected, the values of the scans of polished surfaces #2 and #3 are essentially the same, and the largest intra-scan difference of β_b is only about 5×10^{-3} cm^{-1}, indicating the homogeneity of the bulk Ti:sapphire crystal in the imaging area outside the micro-bubble region. Fig. 6a, corresponding to polish #1, however, shows somewhat enhanced lateral β_b inhomogeneity, which be due to our inability to fully deconvolute bulk and surface optical effects at every coordinate location for the crystal pair with heavy surface damage. The origin of this problem lies either with the possibility that the thick and thin crystal surfaces did not have very well controlled (and therefore quantitatively different) surface damage, and/or with our inability to sample the signal experimentally at precisely the same coordinate points in both crystals. This latter requirement is implicit in using Eqs. (1) and (2) for the extraction of $\beta_b(x, y)$ and $A_s(x, y)$, where both β_b and A_s are assumed to be ideally identical for both crystals. In view of the cutting of both crystals from the same Ti:sapphire rod, only the identity of β_b could be guaranteed, but not that of A_s. Therefore, the bulk and surface absorption deconvolutions might not yield the (ideally) identical data for every point in the imaging region of the crystal with polish #1.

The surface absorptance for all three polishes gradually decreases as the y coordinate increases in Fig. 7.

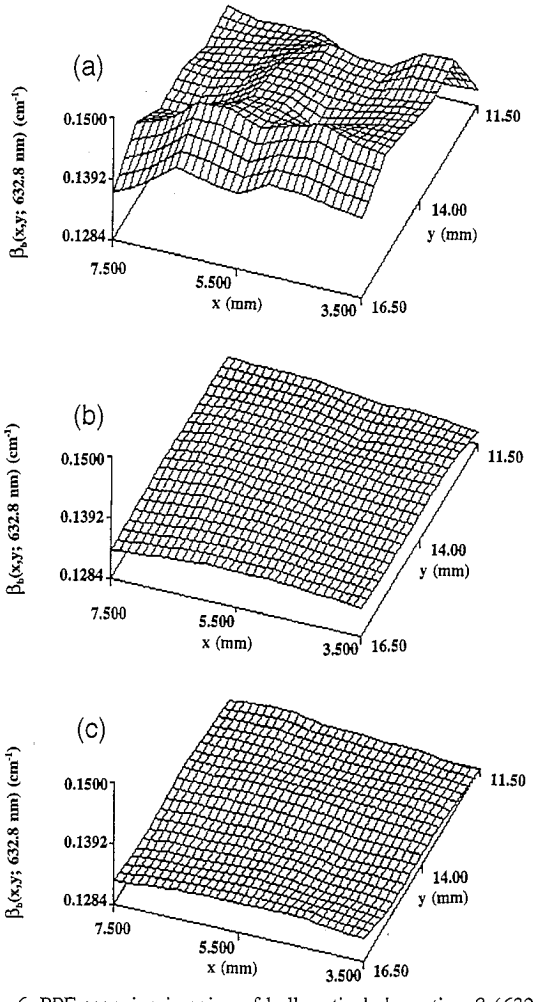

Fig. 6. PPE scanning imaging of bulk optical absorption β_b(632.8 nm) of the Ti:sapphire crystal with (a) polish #1, (b) polish #2, and (c) polish #3.

For polish #1 the surface layer was relatively thick but of unknown thickness and degree of inhomogeneity. For polishes #2 and #3, even though the surface-layer thicknesses were unknown, they were much more homogeneous than polish #1 and much thinner than the samples themselves. Nevertheless, the surface layer plays a dominant role in terms of absorptance, and a very important role in terms of the optical homogeneity of a thin Ti:sapphire laser crystal, especially when the crystal is of high quality: In terms of relative absorptances, Fig. 5 indicates that the bulk absorptance of the 2-mm-thick Ti:sapphire disk at 632.8 nm was $\sim2\times10^{-2}$. At the same wavelength the surface absorptance of the disk with polish #1 was $\sim1.3\times10^{-1}$, and $\sim7.4\times10^{-2}$ with polishes #2 and

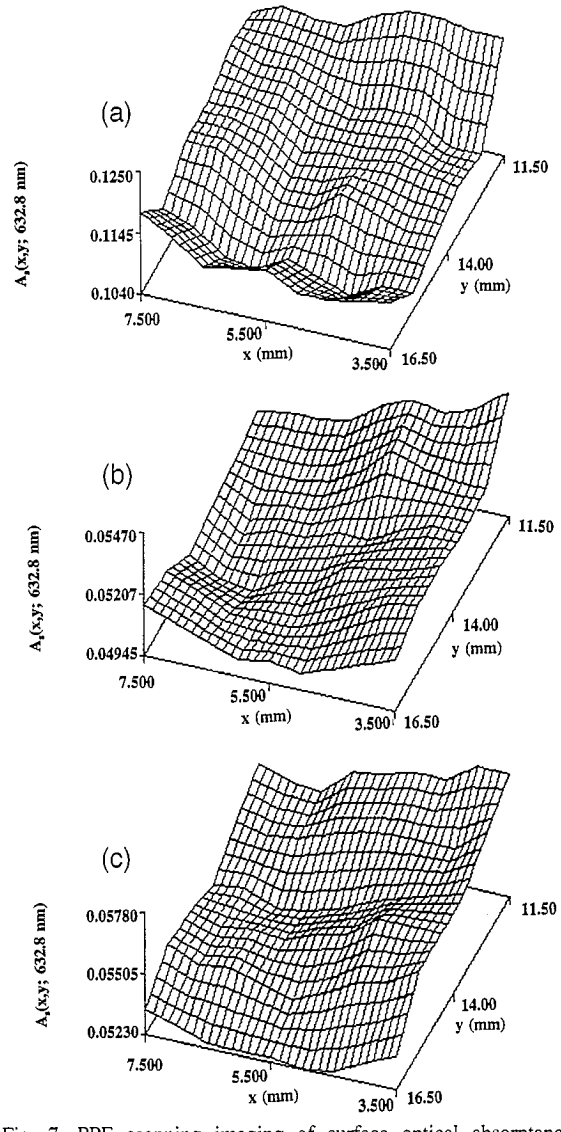

Fig. 7. PPE scanning imaging of surface optical absorptance A_s(632.8 nm) of the Ti:sapphire crystal with (a) polish #1, (b) polish #2, and (c) polish #3.

#3. Fig. 7 clearly indicates the highly defective nature of polish #1 as compared to polishes #2 and #3: not only is the surface absorptance of polish #1 much higher than that of polishes #2 and #3, but also the intra-scan differences of surface absorptance (maximum 2×10^{-2}) of polish #1, are larger than those (maximum 5×10^{-3}) of polishes #2 and #3, indicative of the roughness and inhomogeneity of polish #1.

Fig. 8 presents *theoretically* normalized quadrature signals, Q_n, corresponding to the three polishes. Since the quadrature signal is very sensitive to L, the air-layer thickness between the sample and PVDF detector, as well as the bulk optical absorption coefficient $\beta_b(\lambda)$, surface absorptance $A_s(\lambda)$, and bulk and surface optical-to-thermal energy conversion efficiencies, $\eta_{NR}^{(s)}(\lambda)$ and $\eta_{NR}^{(b)}(\lambda)$ [3], all of these variables should be taken into account when comparing one quadrature signal with others. The air-layer thickness could be precisely estimated by measuring quadrature signals versus L and fitting to [1–3]

$$V_L(\lambda) = \frac{C_1[1-\gamma_{gs}Z\exp(-2\sigma_g L)]+C_2[\exp(-\sigma_g L)]}{1-\gamma_{gs}\gamma_{gp}Z\exp(-2\sigma_g L)}, \tag{3a}$$

where

$$\gamma_{ij}\equiv\frac{1-b_{ij}}{1+b_{ij}}; \tag{3b}$$

b_{ij} is the thermal wave coupling coefficient at the interface (i,j) defined as

$$b_{ij}\equiv\frac{k_i\sqrt{\alpha_j}}{k_j\sqrt{\alpha_i}}; \tag{3c}$$

$\sigma_g\equiv(1+i)(\pi f/\alpha_g)^{1/2}$ is the complex thermal diffusion coefficient in air [9]; and

$$Z\equiv\frac{1-\exp(-2\sigma_s l)}{1-\gamma_{gs}^2\exp(-2\sigma_s l)}. \tag{3d}$$

k_j and α_j are the thermal conductivity and thermal diffusivity in material j (= g,s,p, denoting air, Ti:sapphire crystal sample, and PVDF detector, respectively), Fig. 1. C_1 and C_2 are complex constants, which depend on the optical and thermal properties of sample and pyroelectric detector. They are complicated algebraic expressions [3], but they are straightforward for numerical calculations. $\eta_{NR}^{(s)}(\lambda)$ was set equal to 1 (= 100%) based on physical arguments of total nonradiative conversion by the damage-originating NRSLs [3]. Initially setting $\eta_{NR}^{(b)}(\lambda)$ equal to 1, which corresponds to total thermal conversion of all the optical energy absorbed by the sample, one can obtain theoretically the maximum quadrature signal corresponding to a given set of values of L, β_b and A_s. The experimental quadrature signal $S_Q^{(exp)}$ normalized by the theoretical one $S_Q^{(th)}$, Eq. (2),

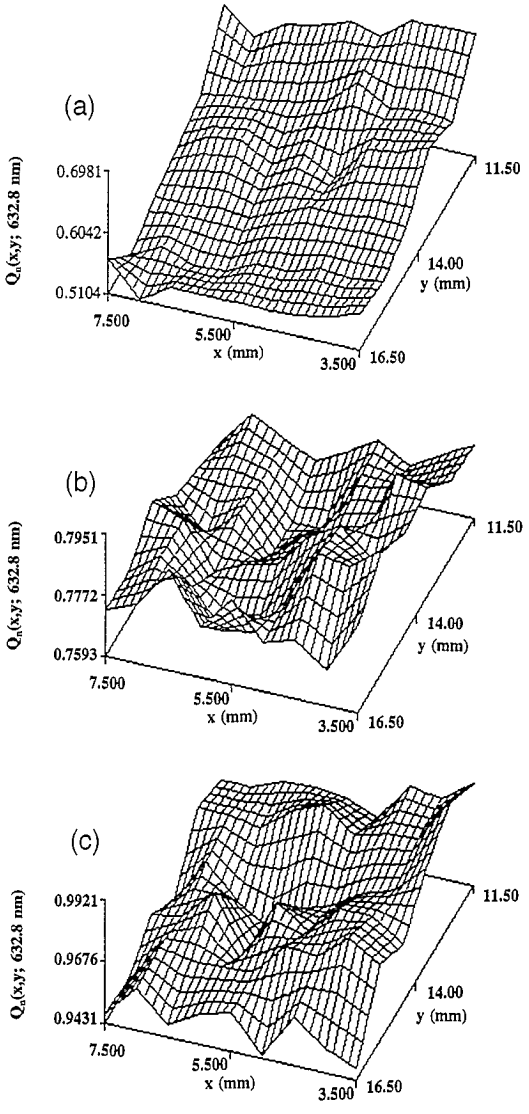

Fig. 8. PPE scanning imaging of normalized quadrature signals, $Q_n(632.8\ nm)$, Eq. (4) of the Ti:Sapphire crystal with (a) polish #1, (b) polish #2, and (c) polish #3.

$$Q_n(\lambda) \equiv \frac{S_Q^{(exp)}(\lambda)}{S_Q^{(th)}(\lambda)}, \tag{4}$$

is a measure of the degree of optical-to-thermal energy conversion of the sample. It should be noted that the scanned image of $\eta_{NR}^{(b)}(x, y)$ is not as useful a crystal-quality characterization parameter as $Q_n(x, y)$: The former quantity gives information on the fraction of incident optical energy *per absorption center*, which is converted into thermal energy locally per duty cycle. The latter quantity, however, gives the *total amount* of thermal energy per duty cycle released by all absorbing (and energy converting) local centers within the interaction volume V of the exciting incident radiation. Therefore, $Q_n(x, y)$ yields a more useful measure of the energy conversion characteristics of the scanned crystalline regions, as it involves the probability of optical-to-thermal energy conversion events *and* the density $N(x, y)$ of energy conversion centers within the interaction volume. This latter effect is normalized out in the $\eta_{NR}^{(b)}(x, y)$ scan. One may thus write:

$$Q_n(x, y) \equiv \eta_{NR}^{(b)}(x, y)\ N(x, y)\ V. \tag{5}$$

For our particular samples, Fig. 8 shows that Q_n increases with surface polish in the direction from polish #1 to #3. Such changes are artifacts due to the effects of different polishes, since $\eta_{NR}^{(b)}$ should be the same for the same crystal. In a photopyroelectric experiment, the rear sample surface layer is the closest to the PVDF detector; only the thermal wave generated in a thin layer close to the rear surface in the bulk crystal on the order of a few thermal diffusion lengths (ca. 0.6 mm in Ti:sapphire, at $f = 9$ Hz) can communicate with the detector [3]. The rear surface layer plays two roles: (a) it forms a thermal resistance proportional to its thickness; thus a thermally thick [9] rear surface layer attenuates the thermal wave produced through optical absorption in the bulk; and (b) it generates heat whenever it absorbs optical energy, thus becoming a localized heat source. These two effects act in opposite directions, with the former mechanism tending to *decrease* the magnitude of the transmitted thermal wave, and the latter mechanism tending to *increase* it. In the case of our experimental geometry as shown in Fig. 1, the more the front surface absorbs, the less optical energy is transmitted into the crystal, and thus the less heat is produced in the rear surface layer and the thin bulk layer adjacent to it. Among the three polishes, #1 was the thickest and most opaque, inducing the lowest Q_n, as the combined result of the smaller thermal wave power released into the optically transparent bulk of the crystal due to diminished transmission through the damaged front surface layer, and the attenuation of thermal waves due to the (likely thermally thick) rear surface layer. The same reasoning can be applied to polish #2 to explain the lower Q_n than that of polish #3. While surface optical absorptances of polishes #2 and #3 at 632.8 nm are more or less the same, as shown in Figs. 5b and 7b, c, the surface layer

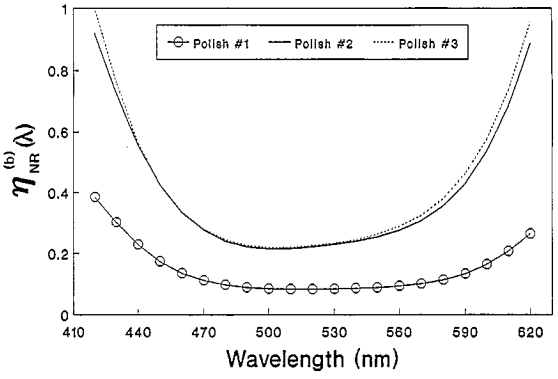

Fig. 9. Nonradiative energy-conversion-efficiency spectra of Ti:sapphire thin crystal with polishes #1–3.

with polish #2, which was thicker than that of polish #3, appears to have higher thermal resistance (lower thermal conductivity) than that of polish #3, resulting in lower Q_n.

Consistent with the foregoing findings are also the spectra of the effective nonradiative energy conversion efficiency, $\eta_{NR}^{(b)}(\lambda)$, obtained from the Ti:sapphire crystal with each of the polishes #1–3, Fig. 9, using Eq. (2). The effective $\eta_{NR}^{(b)}(\lambda)$ for the heavily damaged layer #1 is lower than that corresponding to the other two polishes and this is an artifact of the surface thermal resistance layer. The near coincidence of the $\eta_{NR}^{(b)}(\lambda)$ spectra for polishes #2 and #3 indicates that the Q-signal normalization, $S_Q(\lambda)$, was adequate to deconvolute the (constant) behavior of the bulk from the variations in the surface polish layer. The absolute values of $\eta_{NR}^{(b)}(\lambda)$, as well as its spectral lineshape, have been dealt with elsewhere [3,10]. The comparison between the nearly identical $\eta_{NR}^{(b)}(\lambda)$ spectra #2 and #3 in Fig. 9 and the more pronounced variations between Q_n in Figs. 8b,c, shows that the differences must be sought in the fact that Q_n is also sensitive to the total number of energy converting centers in the bulk, as indicated by Eq. (5). Therefore, this comparison provides an additional justification for the use of $Q_n(x, y)$, rather than $\eta_{NR}^{(b)}(x, y)$ PPE scanning imaging for the purposes of optical quality characterization of laser materials.

The foregoing analysis is further consistent with independent experiments using infrared photothermal radiometric measurements performed in this laboratory. It was found that the thermal wave contributions from the surface polish layers varied from large to small in the order of polishes #1, 2 and 3, thus indicating that the surface thermal power retention (a measure of thermal resistance) changed from high to low as polishes changed from #1 to #3. The importance of Fig. 8 lies in the fact that thermal resistance of the surface layer will potentially prevent to various degrees the Ti:sapphire crystal from dissipating heat when lasing in an optical resonator cavity. It is also a measure of surface optical quality, since surface damage reabsorbs emission luminescence, thus reducing the quantum efficiency. In comparing the usefulness of purely optical PPE scans of Ti:sapphire crystals, such as those shown in Figs. 6 and 7, as optical quality control scanning imaging, with the photothermal scans of Fig. 8, it can be seen that the purely optical scans are *less* sensitive to variations between polish #2 and #3. Based on the purely optical scans, both polishes #2 and #3 are almost equally acceptable (polish #3 is the industrial standard at Crystar Research Inc.). The thermal-wave scans of Fig. 8, however, are more sensitive to the presence of surface damage and clearly indicate the improved quality of polish #3, higher by ~20% than polish #2.

4. Conclusions

Photopyroelectric scanning imaging of a Ti:sapphire crystal with three deferent polishes has been carried out to obtain bulk optical absorption coefficient, surface absorptance and normalized lock-in amplifier quadrature signal images. These images were consistent with the roughness, inhomogeneity, high surface absorption and large thermal resistance of the surface with polish #1. They also clearly differentiated between the photothermal quality of the surface with polish #2, which appeared to have higher thermal resistance than that of the best polish #3. The respective purely optical images obtained using scanning PPE IP-imaging showed little difference between the surface with polish #2 and #3. Scanning PPE Q-imaging therefore provides a useful tool for non-destructive, non-contact monitoring of the quality of Ti:sapphire polished crystal surfaces.

Acknowledgements

We gratefully acknowledge a Strategic Grant from the Natural Sciences and Engineering Research Coun-

cil of Canada (NSERC), which made this work possible.

References

[1] A. Mandelis, J. Vanniasinkam, S. Buddhudu, A. Othonos and M. Kokta, Phys. Rev. B1 48 (1993) 6808.
[2] S. Buddhudu, J. Vanniasinkam, A. Mandelis, B. Joseph and K. Fjeldsted, Opt. Mater. 3 (1994) 115.
[3] J. Vanniasinkam, A. Mandelis, S. Buddhudu and M. Kokta, J. Appl. Phys. 75 (1994) 8090.
[4] H.S. Carslaw and J.C. Jaeger, Conduction of Heat in Solids, 2nd Ed. (Oxford, 1959) Chap. 2.6.
[5] D.S. McClure, J. Chem. Phys. 36 (1962) 2757.
[6] P. Lacovara, L. Esterowitz and M. Kokta, IEEE J. Quantum Electron. QE-21 (1985) 1614.
[7] M.R. Kokta, in: Proceedings of the OSA Topical Meeting, eds. A.B. Budgor, L. Esterowits and L.G. DeShazer (New York, 1986) p. 89.
[8] G.F. Albrecht, J.M. Eggleston and J.J. Ewing, in: Tunable Solid State Lasers, eds. P. Hammerling, A.B. Budgor and A. Pinto (New York, 1985) p. 68.
[9] A. Mandelis and M. Zver, J. Appl. Phys. 57 (1985) 4421.
[10] M. Grinberg and A. Mandelis, Phys. Rev. B1 49 (1994) 12496.